UDC 551.509.313 551.521.32: 535-1

A SIMPLE METHOD OF INCLUDING LONGWAVE RADIATION IN A TROPOSPHERIC NUMERICAL PREDICTION MODEL [1]

MAURICE B. DANARD
Naval Postgraduate School, Monterey, Calif.[2]

ABSTRACT

A simple method of computing longwave radiative cooling in the troposphere associated with water vapor is described. The procedure may readily be incorporated into a tropospheric numerical prediction model. Radiation from ozone and carbon dioxide is not considered. However, influences of arbitrary vertical distributions of cloud and moisture are included.

Average annual cooling rates along a meridional cross section are calculated for a cloudless atmosphere. The results agree fairly well with the total radiative cooling (longwave and shortwave) as given by Manabe and Möller except in the lower troposphere at low latitudes. Here shortwave absorption by water vapor is appreciable.

The three-dimensional distribution of longwave radiative cooling is also computed in a case of a developing cyclone for comparison with that of release of latent heat. The largest cooling occurs at cloud top and can be a significant fraction of the amount of energy released as latent heat in the upper troposphere. Computations also show that in this case study the longwave cooling tends to reduce the available potential energy, especially in the upper troposphere.

Synoptic-scale precipitation amounts resulting from destabilization of clouds by longwave cooling are computed. These range up to 1.4 mm in 12 hr. This destabilizing effect may be important in explaining the nocturnal maximum of precipitation over the sea. It may also contribute significantly to cyclone development.

1. INTRODUCTION

The heat budget of the atmosphere may be partitioned as follows: 1) sensible heat transfer from the earth's surface by conduction and convection, 2) absorption of shortwave radiation, 3) release of latent heat, and 4) absorption and emission of longwave radiation. Of these, longwave radiation is the most important term in the mean tropospheric heat budget (see, e.g., Davis, 1963, or London, 1957). Release of latent heat is, on the average, the second most important term. However, it is often locally predominant in areas of precipitation and its inclusion in a prediction model appears desirable in forecasting cyclogenesis (Danard, 1964, 1966a, 1966b).

Using a numerical model incorporating release of latent heat but not longwave radiation, the author (Danard, 1966a, 1966b) noted a tendency for predicted heights to be too high in the upper troposphere. This may have been due to neglect of longwave cooling from cloud tops. Inclusion of longwave radiation should extend the viability of such models.

Flux divergence associated with carbon dioxide is usually small in the troposphere (see, e.g., Manabe and Möller, 1961, or Manabe and Strickler, 1964). Mean hemispheric cooling rates below 12 km for a cloudless atmosphere may be estimated from figure 22 of Manabe and Möller (1961). These amount to about 1.2°C day^{-1} for longwave radiation from water vapor compared to only 0.2°C day^{-1} for carbon dioxide. Therefore, only water vapor will be considered.

Sections 2 and 3 of this paper describe a simple method of including longwave radiation from water vapor in a tropospheric numerical model that predicts the field of moisture. Effects of arbitrary vertical distributions of cloud and moisture are included.

In section 4, computations using the above method for a mean Equator to Pole cross section with clear skies are presented. Results agree reasonably well with those of Manabe and Möller (1961).

Section 5 compares the three-dimensional distributions of longwave radiative cooling and release of latent heat in a synoptic case study. Released latent heat is an order of magnitude larger than longwave cooling in the region of the cyclone. Longwave radiative cooling is appreciable at cloud top.

Calculations of Katayama (1967) show that longwave radiation, absorption of solar radiation, and release of latent heat are about equally important in the annual mean generation of available potential energy over the Northern Hemisphere. Section 6 is concerned with the

[1] A summary of much of this paper was presented at the Annual Congress of the Canadian Meteorological Society held in Calgary, Alberta, June 3–5, 1968.

[2] Present affiliation, Department of Mechanical Engineering, University of Waterloo, Ontario.

first of these processes. Computations are performed for the same synoptic case as in section 5. Cloud top cooling reduces temperature contrasts if the cloud mass is in the warm air.

The existence of a nocturnal maximum in frequency of precipitation over the sea has been demonstrated by Kraus (1963). He studied the records of weather ships in the eastern Pacific and north Atlantic Oceans. With 8–10 yr of data for July, he found that precipitation was reported in 19% of all nocturnal reports compared to 12% of the daytime reports. Kraus proposed that during the day absorption of shortwave radiation reduces the production of liquid water in clouds, thereby lowering the probability of precipitation. At night, this effect is absent.

The nocturnal maximum in precipitation occurrence over the central United States in summer was studied by Bleeker and Andre (1951). Their explanation was that low level differential cooling at night due to variations in topography would result in upward motion between the Appalachians and the Rockies.

In section 7 it is suggested that an important factor in nocturnal precipitation is the destabilizing influence of longwave cooling from cloud top. The amount of precipitation associated with convective overturning is computed. The destabilization would likely also augment the large-scale vertical velocity. This would further increase the precipitation as well as accelerate cyclone development.

2. COMPUTATION OF LONGWAVE RADIATION FROM WATER VAPOR

Computations will be performed for the atmosphere below some level p_u (near the tropopause). This is the highest level for which meteorological variables are assumed known.

Results of Kuhn (1963c) suggest the following expression for the corrected precipitable water or path length between $p=0$ and $p=p$:

$$w=\frac{1}{g}\int_0^p q\left\{\frac{p}{p_0}\right\}^{0.85}\left\{\frac{T_0}{T}\right\}^{0.5}dp. \tag{1}$$

Here p_0 and T_0 denote standard pressure and temperature, q is the specific humidity, and w may be regarded as a vertical coordinate increasing downward.

In computing w_u, the value of w at $p=p_u$, use is made of Manabe and Möller's (1961) observation that the frost point in the lower stratosphere is about 190°K irrespective of season and latitude. This value is attained at a height of about 15 km or 120 mb. The frost point is more or less constant above this level. Assume that the layer above p_u is isothermal with temperature T_u. Setting $T_u=220$°K, (1) then gives a value for w from $p=0$ to $p=120$ mb of 4.6×10^{-7} gm cm $^{-2}$. Assume that q varies linearly with pressure from $p=120$ mb to $p=p_u$. With the aid of (1), this permits us to compute the contribution to w from the layer between these levels. For $p_u=200$ mb,

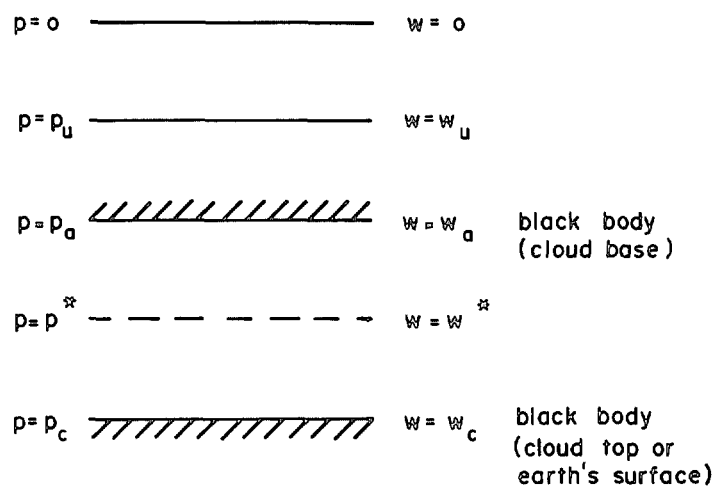

FIGURE 1.—Schematic diagram showing levels referred to in equation (3).

the path length from $p=0$ to $p=p_u$ is (in cgs units)

$$w_u=4.7\times10^{-5}+9.9q_u \tag{2}$$

where q_u is the value of q at $p=p_u$. Note that w_u normally decreases from Equator to Pole.

The net flux (positive downward) at a level p^* between cloud layers (see fig. 1) is

$$F^*=F_{ba}-F_{bc}+\int_{w_a}^{w^*}\{F_{bw}-F_{ba}\}\epsilon'(w^*-w)dw + \int_{w^*}^{w_c}\{F_{bc}-F_{bw}\}\epsilon'(w-w^*)dw \tag{3}$$

where F_{bw}, F_{ba}, and F_{bc} are the black-body fluxes corresponding to the temperature at w, w_a, and w_c, and $\epsilon'(w^*-w)$ is the rate of change of emissivity ϵ with path length evaluated at a path length (w^*-w) (corresponding to the slab between w and w^*). Throughout this paper, arguments of functions are enclosed in parentheses ( ). A similar equation is given by Kuhn (1963c). If the level p^* is in cloud, F^* is assumed zero. If no cloud exists above p^*, $w_a=0$ and $F_{ba}=0$. Equation (3) is derived in a manner similar to that described by, e.g., Haltiner and Martin (1957, pp. 85–86). An outline of the derivation is given in the remainder of this paragraph. The flux in the spectral interval λ to $\lambda+d\lambda$ at w^* from the black-body surface at w_a is

$$dF^*_{a\lambda}=2E_{a\lambda}d\lambda H_3(k_\lambda\{w^*-w_a\}) \tag{4}$$

where $H_n(x)=\int_0^\infty e^{-xy}y^{-n}dy$, $E_{a\lambda}d\lambda$ is the black-body flux at w_a in the spectral interval λ to $\lambda+d\lambda$ (i.e., $\int_0^\infty E_{a\lambda}d\lambda=F_{ba}$), k_λ is the absorption coefficient and λ is the wavelength. The flux at w^* from the stratum between w_a and w^* is

$$dF^{*\downarrow}_{w\lambda}=2k_\lambda\int_{w_a}^{w^*}E_{w\lambda}d\lambda H_2(k_\lambda\{w^*-w\})dw \tag{5}$$

where $E_{w\lambda}d\lambda$ is the black-body flux at w in the spectral interval λ to $\lambda+d\lambda$. Now

$$H_3(k_\lambda\{w^*-w_a\})=\frac{1}{2}-k_\lambda\int_{w_a}^{w^*}H_2(k_\lambda\{w^*-w\})dw. \quad (6)$$

Adding (4) and (5), making use of (6), and integrating over all wavelengths yields

$$F^{*\downarrow}=F_{ba}-2\int_{w_a}^{w^*}\int_0^\infty k_\lambda E_{a\lambda}H_2(k_\lambda\{w^*-w\})d\lambda\,dw +2\int_{w_a}^{w^*}\int_0^\infty k_\lambda E_{w\lambda}H_2(k_\lambda\{w^*-w\})d\lambda\,dw. \quad (7)$$

Now for an isothermal slab,

$$\epsilon'(w^*-w)=\frac{2}{F_{bw}}\int_0^\infty k_\lambda E_{w\lambda}H_2(k_\lambda\{w^*-w\})d\lambda. \quad (8)$$

Equation (8) is derived by, e.g., Brooks (1950). It may also be obtained from (5). For a fixed value of (w^*-w), ϵ and therefore ϵ' as well will be assumed independent of temperature. This is because the temperature dependence has already been included in (1), which is used to compute w and w^*. Hence (8) will be assumed to apply also when the temperature varies between w and w^*. Thus the last term on the right side of (7) is $\int_{w_a}^{w^*}F_{bw}\epsilon'(w^*-w)dw$. Making the approximation $E_{a\lambda}d\lambda/F_{ba}=E_{w\lambda}d\lambda/F_{bw}$ (i.e., for fixed λ and $d\lambda$, $E_\lambda d\lambda/F_b$ is assumed to vary little over the range of tropospheric temperatures), the second term on the right side of (7) becomes $-F_{ba}\int_{w_a}^{w^*}\epsilon'(w^*-w)dw$. Hence (7) gives the first and third terms on the right side of (3). Similar calculations show that the contributions from the black-body surface at w_c, and the layer between w^* and w_c are represented by the second and final terms on the right of (3).

The assumption that a cloud surface behaves as a black body is probably justified for water droplet clouds at low elevations. For example, Kuhn (1963c) measured the emissivity of an overcast stratocumulus cloud deck with base at 900 mb and top at 855 mb. He obtained the value of 0.98. As Kuhn's results indicate, however, the assumption is less realistic for clouds at higher elevations. For a 9/10 sky cover of cirrostratus with base at 235 mb and top at 160 mb, the computed emissivity was 0.59.

The heating rate associated with radiation is given by

$$\left(\frac{\partial T}{\partial t}\right)_r=-\frac{g}{c_p}\frac{\partial F^*}{\partial p}. \quad (9)$$

3. ADAPTATION TO A NUMERICAL MODEL

For purposes of illustration, the model described in section 2 will be adapted to a primitive equations numerical model developed by Krishnamurti (manuscript in preparation). However, it could be modified to any model in which a moisture parameter is predicted.

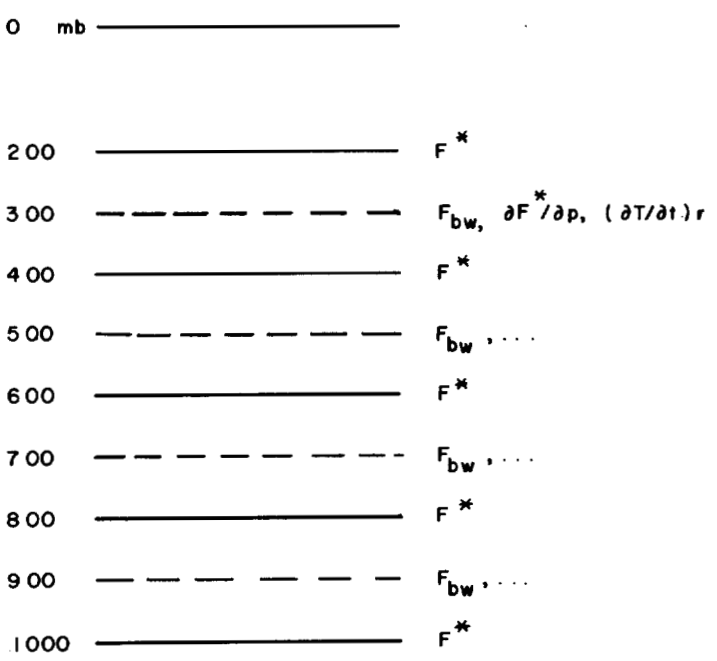

FIGURE 2.—Schematic diagram showing levels at which terms in equations (3) and (9) are computed in section 3.

The level p_u is taken as 200 mb and equation (2) is used to compute w_u. Equation (3) is evaluated at 200, 400, 600, 800, and 1000 mb (fig. 2). The integrals are computed by summation over 200-mb-thick layers. For example,

$$\int_{w_a}^{w^*}\{F_{bw}-F_{ba}\}\epsilon'(w^*-w)dw=\Sigma\{\overline{F}_{bw}-F_{ba}\}\{\epsilon(w^*-w_t)-\epsilon(w^*-w_b)\}. \quad (10)$$

Here w_t and w_b are the values of w at the top and bottom of the 200-mb-thick contributing layer, and $\overline{F}_{bw}$ is the black-body flux at the midpoint. The summation extends over all layers between w_a and w^*. Similarly,

$$\int_{w^*}^{w_c}\{F_{bc}-F_{bw}\}\epsilon'(w-w^*)dw=\Sigma\{F_{bc}-\overline{F_{bw}}\}\{\epsilon(w_b-w^*)-\epsilon(w_t=w^*)\}. \quad (11)$$

In (11), the summation extends over layers between w^* and w_c. Kuhn (1963a) employed a similar method of computation.

Cloud is assumed to exist at a given level if

$$q/q_s>r(p) \quad (12)$$

where q_s is the saturation specific humidity and $r(p)$ is a critical value for existence of cloud. Table 1 gives values

TABLE 1.—*Values of r(p) (see equation (12)) for existence of cloud (adapted from Smagorinsky, 1960)*

p (mb)	900	700	500	300
$r(p)$	0.84	0.75	0.70	0.69

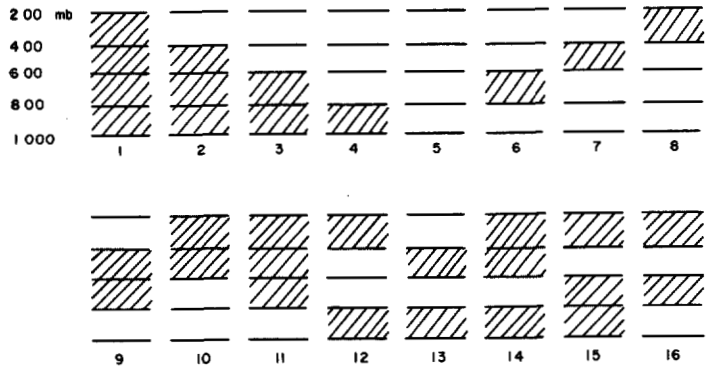

FIGURE 3.—Configurations of cloud in the model atmosphere of section 3. Hatching denotes cloud.

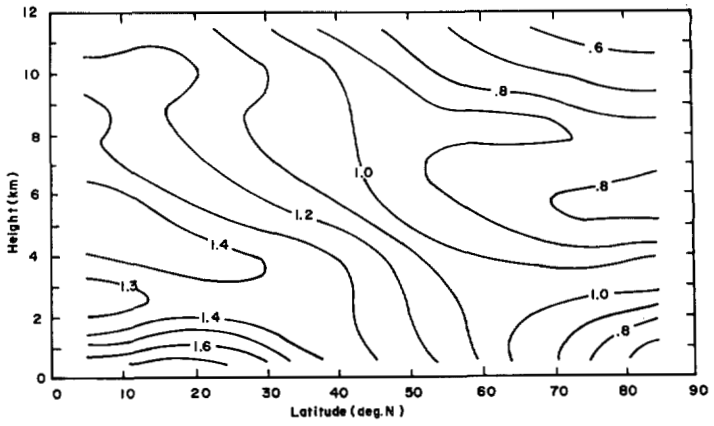

FIGURE 4.—Annual average cooling rates for a cloudless atmosphere associated with longwave radiation from water vapor. Units: °C day^{-1}.

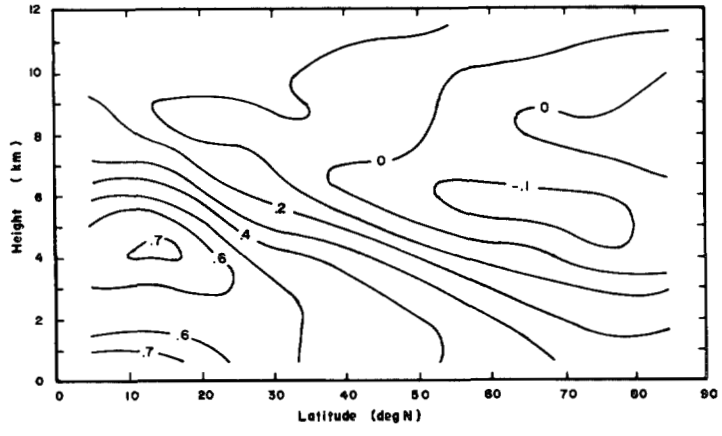

FIGURE 5.—Difference between cooling rates of figure 4 and those of Manabe and Möller (1961), who include both longwave and shortwave radiation. Units: °C day^{-1}.

of $r(p)$ adapted from Smagorinsky's (1960) relations between relative humidity and cloud amount. The values in the table correspond to $\%_0$ cloud at the given level. Relation (12) is tested at 300, 500, 700, and 900 mb, with the cloud (if it exists) corresponding to each level assumed to be 200 mb thick. The model atmosphere can thus have 16 configurations of cloud ranging from completely cloud-free to cloudy at all four levels (fig. 3). Kuhn's (1963b) values of ϵ are used.

In the computer programming of equation (3), F^* is first set equal to zero at the five levels indicated in figure 2. Then it is evaluated from 200 mb down to the top of the highest cloud (or the earth's surface). This means that at this stage flux computations are complete for configurations 1–5 of figure 3. Next, F^* is computed from the base of the highest cloud down to the top of the next highest cloud (or the earth's surface). This completes calculations for configurations 6–15. Finally, F^* is computed at the 800- and 1000-mb levels of configuration 16 to finish the flux computations.

Equation (9) is evaluated at 300, 500, 700, and 900 mb by expressing $\partial F^*/\partial p$ as a finite difference over layers 200 mb thick (see fig. 2).

4. APPLICATION TO A MEAN MERIDIONAL CROSS SECTION

Manabe and Möller (1961) compute the annual average cooling rates associated with radiation as a function of height and latitude for the Northern Hemisphere. They include longwave and shortwave absorption by ozone, carbon dioxide, and water vapor and neglect the effects of clouds.

Since only longwave absorption by water vapor is included in the method presented in this paper, it is of interest to compare the tropospheric cooling rates thus computed with those of Manabe and Möller.

Using the mean values of temperature and pressure compiled by London (1957), equation (3) was evaluated at 1-km intervals from the surface to 12 km. London's humidity values were accepted for $T > -30$°C. However, at lower temperatures, a constant frost point lapse rate of 6.25°C km^{-1} was assumed. This was also done by Manabe and Möller. Equation (2) was used to compute w_u and p_u was taken as 200 mb. For comparison with Manabe and Möller's results, the atmosphere was assumed cloud free. Cooling rates were computed at 0.5, 1.5, . . . , 11.5 km. Average annual values, which have been smoothed slightly, are presented in figure 4. Figure 4 may be compared with figure 21 of Manabe and Möller (1961). The two figures are fairly similar. The average cooling rate in figure 4 is 1.1°C day^{-1} compared to 0.9°C day^{-1} for Manabe and Möller's results for the same region. Differences between the results of this paper and those of Manabe and Möller may be seen in figure 5. It will be seen that considering just longwave radiation from water vapor tends to overestimate the total radiative cooling (longwave and shortwave) at low latitudes and low levels. The discrepancy is probably due to shortwave absorption by water vapor. Results of Davis (1963) indicate that in such regions this absorption can be half as large as the longwave cooling.

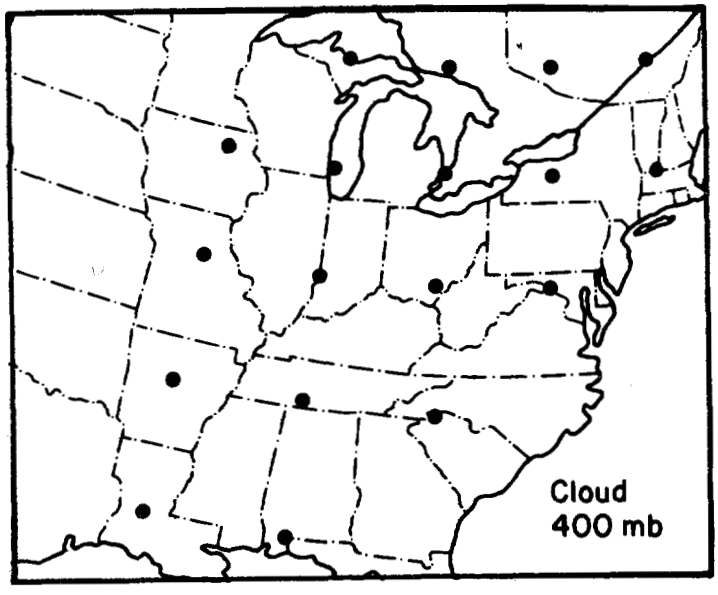

FIGURE 6.—Gridpoints at which cloud exists at 400 mb. 1200 GMT Jan. 21, 1959.

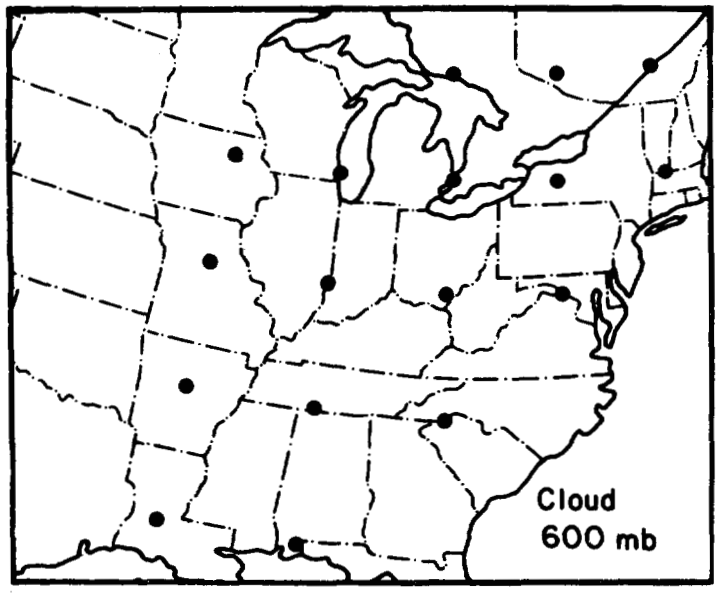

FIGURE 7.—As in figure 6 but for 600 mb.

Note that the above comparison is not simply a test of the method used to compute longwave radiation from water vapor. It is primarily an assessment of the validity of omitting shortwave radiation as well as longwave radiation from carbon dioxide and ozone in the troposphere.

Figure 4 may also be compared with the infrared cooling rates of London (1957). However, London accounted for average cloudiness whereas in the present study the atmosphere was assumed cloud free.

Figure 22 of Manabe and Möller (1961) gives a mean cooling rate of 1.2°C day^{-1} for longwave radiation from water vapor. By comparison, the value obtained in this paper is 1.1°C day^{-1}. Goody (1964, p. 272) states that cooling rates computed from different techniques may vary by as much as 50%. Therefore, the agreement with Manabe and Möller's results must be considered as reasonably good.

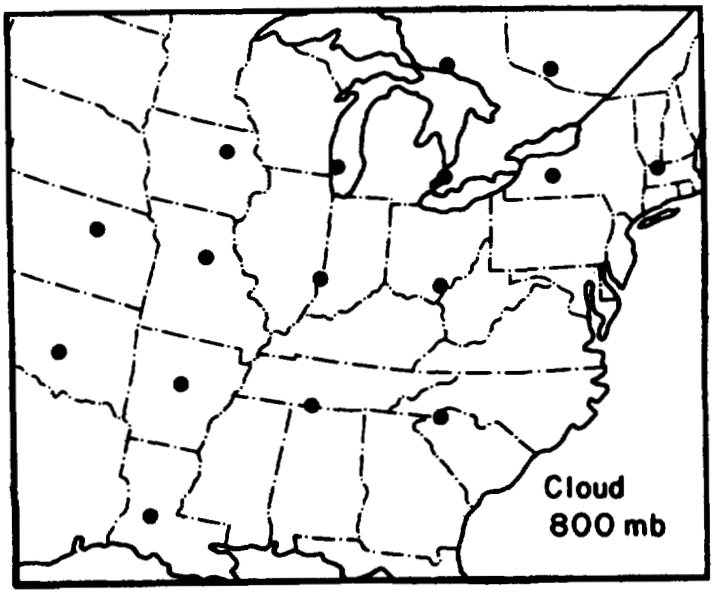

FIGURE 8.—As in figure 6 but for 800 mb.

5. COMPARISON WITH RELEASE OF LATENT HEAT

The author has previously calculated the three-dimensional distribution of release of latent heat at 400, 600, and 800 mb in a developing cyclone over the United States (Danard, 1964). To permit a comparison between these results and longwave radiative effects, the method described in section 3 was modified somewhat. The level p_u was taken as 300 mb, and T_u was assigned the value 230°K. An equation similar to (2) but applicable here is

$$w_u = 5.0 \times 10^{-5} + 28\, q_u. \tag{13}$$

The 900-mb surface was assumed to be a black body. Equation (3) was then evaluated at 300, 500, 700, and 900 mb, and cooling rates were computed at 400, 600, and 800 mb. Existence of cloud at these levels was deduced using values of $r(p)$ (see (12)) obtained in the same manner as those in table 1. Surface observations were also utilized to verify the presence of clouds. In other respects, the procedures of section 3 were followed. The reader is referred to the paper cited above (Danard, 1964) for synoptic charts and other details of the case studied.

Results are presented in figures 6–12. Figures 6–8 show the grid points at which cloud was deduced to exist. The remainder of the region (see figures 9–12) was essentially cloud free.

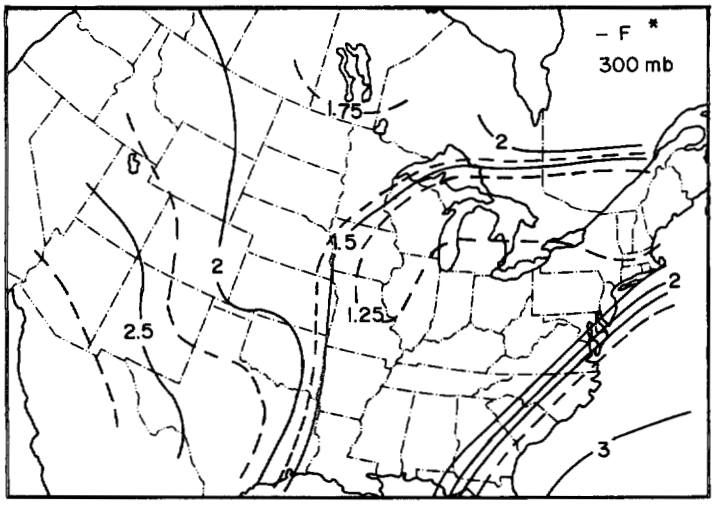

FIGURE 9.—Net upward flux at 300 mb, 1200 GMT, Jan. 21, 1959. Units: 10^5 ergs sec^{-1} cm^{-2}.

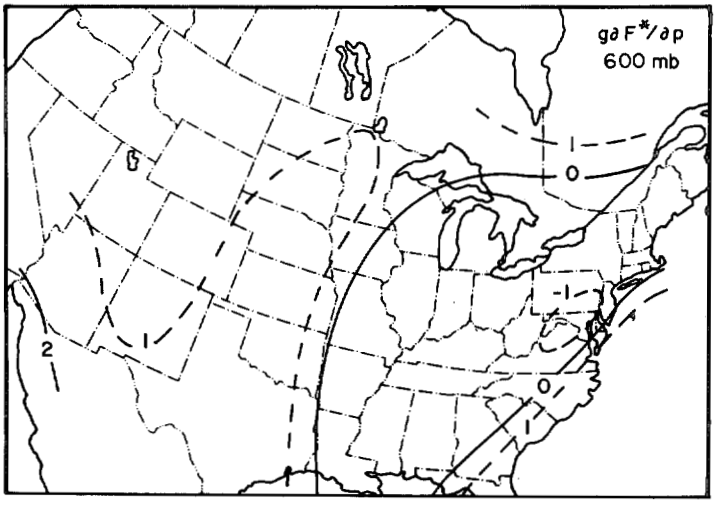

FIGURE 11.—As in figure 10 but for 600 mb.

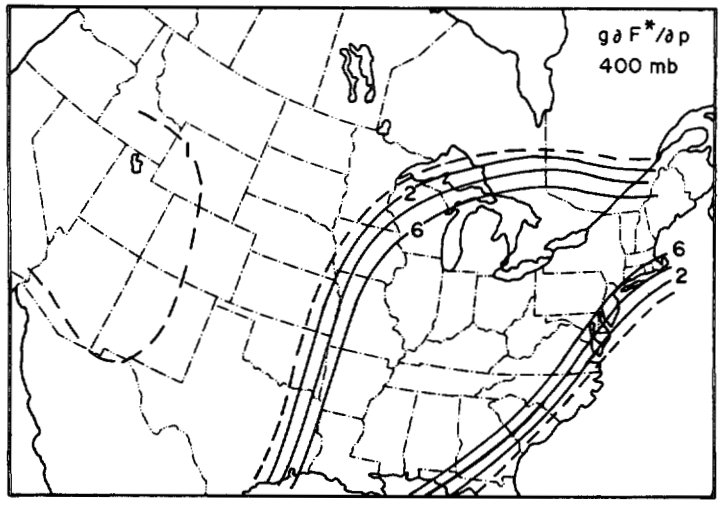

FIGURE 10.—Net loss of radiative energy per unit mass at 400 mb, 1200 GMT, Jan. 21, 1959. Units: 10^2 ergs gm^{-1} sec^{-1}. 1°C day^{-1} $=1.17\times10^{-2}$ ergs gm^{-1} sec^{-1}.

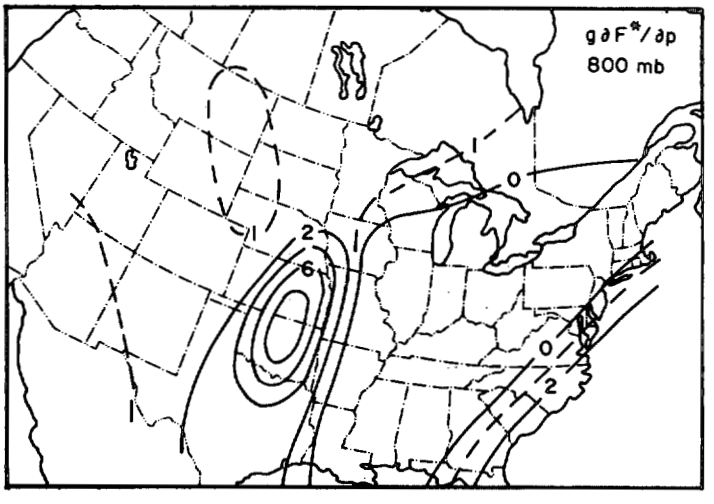

FIGURE 12.—As in figure 10 but for 800 mb.

Figure 9 shows the net flux (positive upward) at 300 mb. The top of the principal cloud deck is clearly delineated by relatively low values of flux. Its lateral boundary is given approximately by the isopleth $F=1.75\times10^5$ ergs sec^{-1} cm^{-2}.

Figures 10–12 show the rate of loss of energy due to longwave radiation from water vapor. By far the greatest loss occurs in the upper portion of the cloud mass. The large values in the Oklahoma-Kansas region at 800 mb (fig. 12) indicate strong cooling at the top of stratocumulus cloud with clear skies above. Zero values mean that the point in question is in cloud. Negative values indicate warming beneath cloud or in the lower portion of the cloud mass. For comparison with the results of section 4, 1°C $day^{-1}=1.17\times10^2$ ergs gm^{-1} sec^{-1}.

Figures 10–12 are to be compared with figure 8 of Danard (1964). The latter depicts the rate of release of latent heat at 400, 600, and 800 mb. This was largest in the Indiana-Pennsylvania area and amounted to about 3×10^3 ergs gm^{-1} sec^{-1} at 400 and 800 mb and about 5×10^3 ergs gm^{-1} sec^{-1} at 600 mb. Thus, in the case studied, the longwave cooling at cloud top was smaller by a factor of about five than the maximum rate of release of latent heat in the upper troposphere. It may be remarked that this case was one of heavy precipitation and in less intense cyclones the ratio would be smaller. However, in the middle and lower troposphere, radiative loss was generally negligible in the region of precipitation compared to release of latent heat.

The longwave cooling at cloud top amounts to 5.4°C day^{-1} in the upper 200 mb of the cloud mass (fig. 10). This latter figure agrees qualitatively with the estimate of Möller (1951). The cooling at cloud top greatly exceeds that in the cloud-free air. Thus an accurate computation

TABLE 2.—*Comparison of terms A and G. See equations (15)–(17).*

Term	Units	900–700 mb	700–500 mb	500–300 mb	900–300 mb
A	10^{25} ergs	6.04	7.36	4.97	18.4
G	10^{20} ergs sec^{-1}	0.26	0.08	−1.66	−1.32
$A/\|G\|$	days	27	104	3.5	16

of the latter may be relatively unessential in the study of cyclogenesis over short time intervals (say 48 hr or less). The longwave cooling would tend to be offset by absorption of solar radiation at cloud top. However, many workers (e.g., Möller, 1951, or London, 1957) regard this effect as small. Nevertheless, this may be important in explaining the diurnal variation of precipitation over the sea (see section 7).

The temperature difference between 800 and 400 mb at the location of the sea level Low (southern Illinois) is 31°C. By comparison, if the lapse rate were pseudoadiabatic, the value would be 34°C. Neglecting effects of vertical motion and differential advection and assuming that the pattern of computed radiative cooling moves with the cyclone, the 800–400 mb temperature difference at the surface Low would be 36°C after 24 hr. This represents a conditionally unstable state which would presumably be alleviated by convective overturning. This problem will be investigated in section 7.

6. EFFECTS OF LONGWAVE RADIATION ON THE AVAILABLE POTENTIAL ENERGY

Consider the thermodynamic energy equation

$$\frac{\partial\alpha}{\partial t}=-\mathbf{V}\cdot\nabla\alpha+\sigma\omega+\frac{RH}{c_p p} \tag{14}$$

where $\sigma=-\alpha\partial \ln\theta/\partial p$, $\omega=dp/dt$, and H is the rate of input of heat per unit mass. In (14), let $\alpha=\bar{\alpha}+\alpha'$, $\sigma=\bar{\sigma}+\sigma'$, etc., where the bar denotes the average over an isobaric surface of area S and the prime the departure therefrom. Equation (14) may then be transformed (Danard, 1966c, or Wiin-Nielsen, 1964) to

$$\frac{\partial A}{\partial t}=-\frac{1}{2g}\int_{p_t}^{p_b}\int_s \mathbf{V}\cdot\nabla\alpha'^2\,dS\,dp+\frac{1}{g}\int_{p_t}^{p_b}\int_s \alpha'\omega'd'\;S\,dp$$
$$+\frac{1}{g}\int_{p_t}^{p_b}\int_s\frac{\alpha'\sigma'\omega'}{\bar{\sigma}}dS\,dp+\frac{R}{c_p g}\int_{p_t}^{p_b}\int_s\frac{\alpha' H'}{\bar{\sigma}p}dS\,dp \tag{15}$$

where

$$A=\frac{1}{2g}\int_{p_t}^{p_b}\int_s\frac{\alpha'^2}{\bar{\sigma}}dS\,dp \tag{16}$$

will be referred to as the available potential energy of the region (cf. equation (10) of Lorenz, 1955, or equation (2.2) of Wiin-Nielsen, 1964). In (15) and (16), p_t and p_b denote the pressures at the top and bottom of the region of interest.

If a quasi-geostrophic balance exists, ω' will be related to H'. However, attention will be restricted here simply to the final term in (15), representing the generation and designated as G:

$$G=\frac{R}{c_p g}\int_{p_t}^{p_b}\int_s\frac{\alpha' H'}{\bar{\sigma}p}dS\,dp. \tag{17}$$

In (17), H' will be identified with longwave radiative effects computed in section 5. The area S is bounded by the latitudes 28.7°N and 51.3°N and by the longitudes 70°W and 115°W (see figs. 9–12). Computations are performed for three layers: 900–700 mb, 700–500 mb, and 500–300 mb. Results are given in table 2.

In the lower layers, G has small, positive values. This is due in large part to the absence of cooling in the lower portion of the main cloud mass (see figs. 11 and 12). In the lowest layer, there is also the effect of cooling from the top of stratocumulus cloud in the cold air over Kansas and Oklahoma (see fig. 12). However, in the uppermost layer, G is negative and fairly large in magnitude. This is due to radiation from cloud top in the warm air. Thus longwave radiation tends to reduce the temperature contrast in the upper troposphere, a not unexpected result. Assuming G constant and neglecting the other terms on the right side of (15), the quotient $A/|G|$ represents the time required to effect a change in A equal in magnitude to the initial value. Whereas this time is of the order of weeks or longer in the lower layers, it is of the order of days in the highest layer. This suggests that longwave radiation from cloud top may be important in the upper troposphere even for short time periods.

7. EFFECTS OF LONGWAVE RADIATION FROM CLOUD TOP ON PRECIPITATION RATES

The basic principles in computing the convective precipitation are similar to those employed by Manabe et al. (1965). Consider an unstable atmosphere initially at rest. If the motions arising from convective overturning are dissipated as heat, it may be shown that

$$\delta\int c_p T\,dm=\int\delta Q\,dm \tag{18}$$

where δ refers to a change over a finite time interval, dm is an element of mass, and δQ is the heat added per unit mass from all sources other than friction. In (18), the integration extends over the entire atmosphere. In a dry adiabatic transformation, the sum of the potential and internal energies (represented by the integral on the left side of (18)) is conserved.

Equation (18) is applied to a layer cloud extending from 1000 to 400 mb. The lapse rate is assumed initially pseudoadiabatic. To simulate conditions during the night, the cloud top radiates for 12 hr. As this proceeds, the cloud becomes unstable. The convective overturning then produces precipitation and returns the lapse rate to the pseudoadiabatic value. The liquid water contents of

TABLE 3.—*Net cooling ($\delta\theta_w$), heat lost by longwave radiation (ΔQ) and total precipitation (P) during 12-hr period for cloud extending from 1000 to 400 mb*

Initial θ_w (°C)	$\delta\theta_w$ (°C)	ΔQ (10^9 ergs cm^{-2})	P (mm)
0	1.2	11.2	0.9
10	0.8	9.8	1.4
20	0.3	6.1	1.4

the initial and final states are assumed equal (i.e., all water which condenses during this process falls out as precipitation).

Applied to the above problem (18) may be written

$$-\frac{c_p}{g}\int_{p_4}^{p_0}\delta T\,dp=\Delta Q+\frac{L}{g}\int_{p_4}^{p_0}\delta r\,dp \tag{19}$$

where p_4=400 mb, p_0=1000 mb, δT (<0), and δr (<0) are the differences between final and initial temperatures and mixing ratios, ΔQ (>0) is the heat lost by radiation, and L is the latent heat of vaporization. The total precipitation is

$$P=-\int_{p_4}^{p_0}\delta r\,\frac{dp}{g}. \tag{20}$$

The interval between p_4 and p_0 is divided into six layers each 100 mb thick. The integrals are then expressed as sums of contributions from these layers. With a known initial state, equation (20) is thus an equation in 12 unknowns, the final values of T and r at the midpoints of the six layers. Eleven more equations are needed. Five are obtained from the final condition that

$$\frac{\partial\theta_e}{\partial p}=0 \tag{21}$$

where

$$\theta_e=\left(T+\frac{Lr}{C_p}\right)\left(\frac{P_0}{p}\right)^{R/c_p} \tag{22}$$

is the equivalent potential temperature. The remaining six equations are obtained from the Clausius-Clapeyron equation. If r_i, e_i, and T_i denote initial mixing ratio, vapor pressure, and temperature, one obtains

$$\delta r=\frac{0.622r_iL}{RT_i^2}\,\frac{p}{p-e_i}\,\delta T. \tag{23}$$

Equation (23) is applied at the six levels.

In computing the radiation lost from cloud top, equations similar to (2) and (13) were derived. The level p_u was taken as 400 mb (cloud top), and q_u was set equal to the saturation value corresponding to the temperature there. The net upward flux at cloud top is thus

$$F_u=F_{bu}(1-\epsilon_u) \tag{24}$$

where F_{bu} is the black body flux corresponding to cloud top temperature, and ϵ_u is the water vapor emissivity for the layer above the cloud. The heat lost by radiation is, per unit area,

$$\Delta Q=F_u\Delta t \tag{25}$$

where Δt=12 hr.

The method described above is applied to three cases where the initial state is saturated with a constant wet bulb potential temperature θ_w of 0°, 10°, and 20°C. These would represent conditions over polar, midlatitude, and subtropical oceans, respectively. Results are shown in table 3.

The values of ΔQ decrease with increasing initial θ_w. This is because the decrease in $(1-\epsilon_u)$ in equation (24) overcompensates the increase in F_{bu}. Release of latent heat tends to offset the cooling due to longwave radiation. This results in fairly small values of $\delta\theta_w$. Precipitation amounts in table 3 are to be regarded as averages over large areas, and not as values associated with individual convective clouds. The amounts increase slightly with initial θ_w. Note that a cooling of only 0.3°C for θ_w=20°C produces more precipitation than does a cooling of 1.2°C for θ_w=0°C.

Precipitation amounts given in table 3 are fairly modest. However, the large-scale vertical velocity has been assumed zero. In a quasi-geostrophic numerical prediction model, the large-scale vertical motion varies inversely as the value assigned to the static stability. Thus the cloud destabilization may lead to an increase in the large-scale vertical velocity also. This would contribute further to the amount of precipitation.

8. CONCLUDING REMARKS

A possible modification to the treatment of clouds would be to allow for fractional amounts in each layer. However, this would complicate the calculations unless the number of layers in the vertical were kept small.

Shortwave absorption by water vapor is appreciable in the lower troposphere at low latitudes (see section 4). This is especially true in summer (see, e.g., Davis, 1963). The average heating due to this source could be included, if desired.

The question of the influence of longwave radiation on the evolution of cyclones is probably best answered by comparative numerical integrations. Although the thermodynamic effects of longwave radiation are usually smaller than those of release of latent heat in cyclones (see section 5), the dynamic influences of the former may still be appreciable. Cooling and destabilization of the upper part of the cloud mass due to radiation are to be expected. If the cloud mass is mainly in the warm air, the cooling

reduces the available potential energy of the region (see section 6). On the other hand, the destabilization leads to convective overturning as well as an increase in the large-scale vertical velocity (see section 7). Destabilization and subsequent increase in precipitation may be important in the dynamics of development.

ACKNOWLEDGMENTS

The author wishes to express his thanks to Professor Frank L. Martin for helpful discussions in the early phases of this study. The research was supported by the U.S. Air Force Cambridge Research Laboratories under Research Project MIPR ES-7-967.

REFERENCES

Bleeker, W., and Andre, M. J., "On the Diurnal Variation of Precipitation, Particularly Over Central U.S.A., and Its Relation to Large-Scale Orographic Circulation Systems," *Quarterly Journal of the Royal Meteorological Society*, Vol. 77, No. 332, Apr. **1951**, pp. 260–271.

Brooks, D. L., "A Tabular Method for the Computation of Temperature Change by Infrared Radiation in the Free Atmosphere," *Journal of Meteorology*, Vol. 7, No. 5, Oct. **1950**, pp. 313–321.

Danard, M. B., "On the Influence of Released Latent Heat on Cyclone Development," *Journal of Applied Meteorology*, Vol. 3, No. 1, Feb. **1964**, pp. 27–37.

Danard, M. B., "On the Contribution of Released Latent Heat to Changes in Available Potential Energy," *Journal of Applied Meteorology*, Vol. 5, No. 1, Feb. **1966***a*, pp. 81–84.

Danard, M. B., "A Quasi-Geostrophic Numerical Model Incorporating Effects of Release of Latent Heat," *Journal of Applied Meteorology*, Vol. 5, No. 1, Feb. **1966***b*, pp. 85–93.

Danard, M. B., "Further Studies With a Quasi-Geostrophic Numerical Model Incorporating Effects of Released Latent Heat," *Journal of Applied Meteorology*, Vol. 5, No. 4, Aug. **1966***c*, pp. 388–395.

Davis, P. A., "An Analysis of the Atmospheric Heat Budget," *Journal of Atmospheric Sciences*, Vol. 20, No. 1, Jan. **1963**, pp. 5–22.

Goody, R. M., *Atmospheric Radiation, Vol. 1. Theoretical Basis*, Clarendon Press, Oxford, **1964**, 436 pp.

Haltiner, G. J., and Martin, F. L., *Dynamical and Physical Meteorology*, McGraw-Hill Book Co., Inc., New York, **1957**, 470 pp.

Katayama, A., "On the Radiation Budget of the Troposphere Over the Northern Hemisphere: III. Zonal Cross-Section and Energy Consideration," *Journal of the Royal Meteorological Society of Japan*, Ser. II, Vol. 45, No. 1, Feb. **1967**, pp. 26–39.

Kraus, E. B., "The Diurnal Precipitation Change Over the Sea," *Journal of Atmospheric Sciences*, Vol. 20, No. 6, Nov. **1963**, pp. 551–556.

Kuhn, P. M., "Soundings of Observed and Computed Infrared Flux," *Journal of Geophysical Research*, Vol. 68, No. 5, Mar **1963***a*, pp. 1415–1420.

Kuhn, P. M., "Radiometersonde Observations of Infrared Flux Emissivity of Water Vapor," *Journal of Applied Meteorology*, Vol. 2, No. 3, June **1963***b*, pp. 368–378.

Kuhn, P. M., "Measured Effective Long-Wave Emissivity of Clouds," *Monthly Weather Review*, Vol. 91, No. 10–12, Oct.–Dec. **1963***c*, pp. 635–640.

London, J., "A Study of the Atmospheric Heat Balance," *Final Report*, Contract No. AF 19(122)-165, Department of Meteorology and Oceanography, New York University, July **1957**, 99 pp.

Lorenz, E. N., "Available Potential Energy and the Maintenance of the General Circulation," *Tellus*, Vol. 7, No. 2, May **1955**, pp. 157–167.

Manabe, S., and Möller, F., "On the Radiative Equilibrium and Heat Balance of the Atmosphere," *Monthly Weather Review*, Vol. 89, No. 12, Dec. **1961**, pp. 503–532.

Manabe, S., Smagorinsky, J., and Strickler, R. F., "Simulated Climatology of a General Circulation Model With a Hydrologic Cycle," *Monthly Weather Review*, Vol. 93, No. 12, Dec. **1965**, pp. 769–798.

Manabe, S., and Strickler, R. F., "Thermal Equilibrium of the Atmosphere With a Convective Adjustment," *Journal of Atmospheric Sciences*, Vol. 21, No. 4, July **1964**, pp. 361–385.

Möller, F., "Long-Wave Radiation," *Compendium of Meteorology*, American Meteorological Society, **1951**, pp. 34–49.

Smagorinsky, J., "On the Dynamical Prediction of Large-Scale Condensation by Numerical Methods," *Geophysical Monograph* No. 5, American Geophysical Union, **1960**, pp. 71–78.

Wiin-Nielsen, A., "On Energy Conversion Calculations," *Monthly Weather Review*, Vol. 92, No. 4, Apr. **1964**, pp. 161–167.

[*Received December 21, 1967; revised August 22, 1968*]

NOTICE OF CHANGE IN "PICTURE OF THE MONTH" SERIES

In January 1963, the *Monthly Weather Review* began publication of a "Picture of the Month." The primary purpose of the series, to acquaint meteorologists and other scientists with the research potential of meteorological satellite information, has by now been well accomplished. Since, however, a number of the published photographs have stimulated successful investigations, the series has been continued, and is now being opened to pictures, not only from satellites but from other sources as well. The basic requirement is that the photographs represent meteorological phenomena of genuine scientific interest and significance. Contributions of such photographs are invited. Pictures should be accompanied by a brief discussion that would normally include data on time, place, camera and film, meteorological conditions, and a description of the feature of interest; weather map analyses, if appropriate, may also be included. Contributions should be limited to one or two printed pages of the *Review*.